THE JOURNAL OF PHYSICAL CHEMISTRY B

ARTICLE

pubs.acs.org/JPCB

Free Energy Calculations of Gramicidin Dimer Dissociation

Surajith N. Wanasundara,[†] Vikram Krishnamurthy,*[,†] and Shin-Ho Chung[‡]

[†]Department of Electrical and Computer Engineering, University of British Columbia, 5500 - 2332 Main Mall, Vancouver, BC, V6T 1Z4 Canada

[‡]Computational Biophsyics, Research School of Biological Sciences, Australian National University, Canberra, ACT 0200 Australia

ABSTRACT:

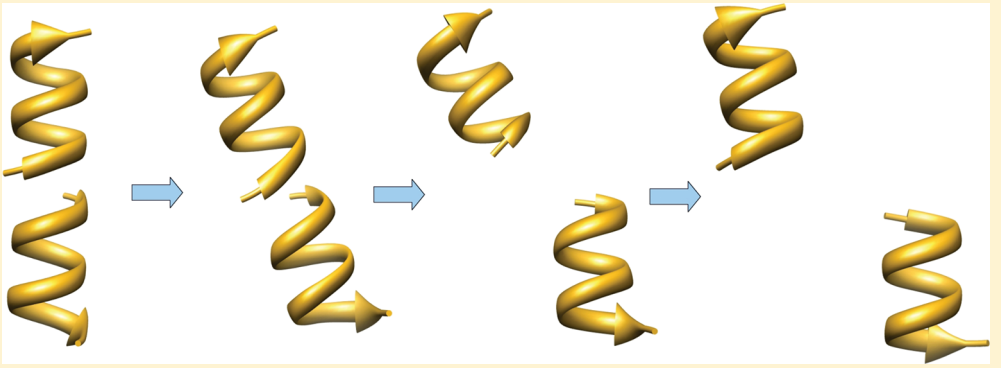

Molecular dynamics simulations, combined with umbrella sampling, is used to study how gramicidin A (gA) dimers dissociate in the lipid bilayer. The potential of mean force and intermolecular potential energy are computed as functions of the distance between center of masses of the two gA monomers in two directions of separation: parallel to the bilayer surface and parallel to the membrane normal. Results from this study show that the dissociation of gA dimers occurs via lateral displacement of gA monomers followed by tilting of dimers with respect to the lipid bilayer normal. It is found that the dissociation energy of gA dimers in the dimyristoylphosphatidylcholine bilayer is 14 kcal mol^{-1} (~22 kT), which is approximately equal to the energy of breaking six intermolecular hydrogen bonds that stabilize the gA channel dimer.

INTRODUCTION

Ion channels are transmembrane proteins, and their function is to regulate the permeability of specific ions across cell membranes. These ion channel proteins are able to serve as key elements in signaling and sensing pathways by connecting the inside and outside of the cell in a selective and gating fashion. They are water-filled narrow pores which have a hydrophilic interior. The channel activation/inactivation or gating involves a series of molecular movements or conformational changes within the protein that opens and closes the pore.[1] Even though different types of ion channels have different characteristics of ion conductance, gating mechanism, and ion selectivity, they all share some distinctive characteristics. Gramicidin A (gA) ion channel, a simple model of ion channels, has been used to study the fundamental principles governing the properties of ion channels since it exhibits some functional similarities to more complex ionic channels.[1] Furthermore, the dynamics of association and dissociation of gA dimers have been used in the implementation of nanoscale biosensors.[2]

Gramicidin A is an antibiotic polypeptide that consists of 15 amino acid residues. Its β-helical, head-to-head (N-terminal-to-N-terminal) dimer in the membranes, stabilized by 6 intermolecular hydrogen bonds, forms a water-filled, ion-conducting pore of about 4 Å diameter that selectively conducts monovalent cations, binds divalent cations, and rejects all anions. The molecular structure of the gA channel, which has been known since the early seventies,[3] has been refined recently to a high-resolution using solid-state[4,5] and liquid-state[6,7] NMR. Its gating involves association and dissociation of gA dimers.[8]

Even though a large number of experimental and theoretical studies have been carried out to investigate the structure, selectivity and permeation of the gA channel,[1,9,10] only few studies involving energy and reaction coordinates of dissociation and association of gA dimer were carried out to understand gating of the gA ion channel. Previous studies showed that dissociation and association rate of gA depends on the hydrocarbon thickness of membrane,[11] voltage,[12] and ion occupancy.[13] Elliott et al.[11] showed that the mean lifetime of gA single channel in a monoacylglycerol bilayer increases as the hydrocarbon thickness of the membrane decreases until it reaches 2.2 nm and becomes approximately constant thereafter. Furthermore, a study conducted by Ring[13] showed that the lifetime of the gA channel increases with permeant ion concentration. Sandblom et al.[12] found that the formation rate of the gA channel rapidly increases with the voltage up to 50 mV. In order to explain the origin of these various phenomena, it is necessary to understand

Received: September 1, 2011
Revised: October 2, 2011

dx.doi.org/10.1021/jp2084583 | J. Phys. Chem. B XXXX, XXX, 000–000

the mechanism of gA dimer dissociation and formation in a lipid bilayer.

Gating processes of gA channels (dissociation/association of dimer) are much slower, typically milliseconds or longer time scale.[11,14] On the other hand, the process may involve multiple transition states and complex dynamics that are not possible or more difficult to capture from experimental studies. Furthermore, recent experimental studies[15,16] show that the gA dimer can exist in multiple conformational states in addition to its conventional open and closed states. Molecular modeling is therefore necessary to understand the gating process. However, only few theoretical studies have been conducted to date in order to get insight of molecular level detail in this process.[17,18] Miloshevsky and Jordan[17,18] have investigated the dissociation pathway of the gA dimer using Monte Carlo methodologies. Miloshevsky and Jordan predicted that the dissociation of the gA dimer involves intermonomer hydrogen bond breaking, backbone realignment, and relative monomer tilt at the intermonomer junction.[18] They further stated that the gA monomers are displaced laterally by ∼4−6 Å, separated by ∼1.6−2.0 Å, and rotated by ∼120° (breaking 2 intermolecular hydrogen bonds) at the transition state of channel dissociation.[17] Due to the simplicity of these models, they may not have captured most of the important dynamics during the dissociation process of the gA dimer in the lipid bilayer/water environment, and more realistic modeling is therefore needed to thoroughly understand this phenomena.

In this study, we combine molecular dynamics (MD) simulations with the umbrella sampling methodology[19] to estimate the dissociation energy of the gA dimer in a lipid bilayer. The potential of mean force (PMF) of the gA dimer was computed as a function of the distance between center of masses (COMs) of two gA monomers in two directions: parallel to the lipid surface (lateral displacement) and parallel to the membrane normal (axial separation). By comparing PMF profiles obtained for lateral displacement and axial separation, the dissociation energy for the gA dimer was then determined. In order to monitor the dissociation process, intermolecular potential energy changes during the dissociation of gA dimer were computed as functions of the lateral displacement and the axial separation.

We show here that the dissociation of gA dimer in the lipid bilayer occurs via an incremental process and the PMF steadily increases as two monomers are displaced laterally until the distance between them reach 1.2 nm, reaching a plateau thereafter. The depth of the PMF is 14 kcal mol^{-1} or 22 kT, which is approximately equal to the energy required to break 6 intermolecular hydrogen bonds.

METHOD

Molecular Dynamics Details. The initial crystal structure of the gA dimer was obtained from the Protein Data Bank (PDB ID: 1MAG).[20] A single gA dimer was inserted into a pre-equilibrated dimyristoylphosphatidylcholine (DMPC) bilayer−water system, obtained from the CHARMM-GUI Web site.[21] The system consists of 128 DMPC molecules (64 in each layer) and 3919 water molecules; thus, the ratio of water to lipid molecules is about 30. The Charmm 27 all-atom force field[22] was used to parametrize the gA and lipid bilayer system. The TIP3P model[23] was used to describe water molecules. Electrostatic interactions were treated using the fast particle-mesh Ewald summation method with cutoff distance at 1.5 nm. The temperature during simulation was kept constant at 313 K by Nosé−Hoover extended ensemble.[24,25] The pressure was maintained at 1 atm in the z direction (parallel to the membrane normal) and −100 atm in the xy plane (parallel to the bilayer surface) by Parinello−Rahman barostat.[26] Negative pressure was applied in xy-plane in order to account for the surface tension in the lipid−water surface.[27] The Gromacs 4 software package[28,29] was used to perform the simulation with a time step of 1 fs. Periodic boundary conditions were applied in all directions.

To remove unfavorable contacts between atoms, the gA dimer−DMPC−water system was first relaxed by energy minimization, followed by 1 ns equilibration MD run with freezing of all atoms in the gA dimer. Then, the system was equilibrated over 3 ns. It should noted that the pore was solvated during the equilibration of the system.

Umbrella Sampling. To determine the free energy profiles, we used the umbrella sampling method.[19] In umbrella sampling, the exploration of phase space relies on MD simulations over a series of regions (windows) that are distributed along a predefined reaction path. Biasing potentials are added to the Hamiltonian to confine the molecular system around the selected regions of phase space. The biasing potential is usually a harmonic potential[19] that keeps the system near a specified value in the reaction path. This is done in a number of windows along the reaction path. In each window, equilibrium simulations are carried out and the biased probability distribution (histogram) is obtained. The weighted histogram analysis method (WHAM)[30] is then used to determine the optimal free energy constants for the combined simulations.

To study how gA channel dissociates in lipid bilayer, the PMF computation was carried out by changing the distance between COMs of the two gA monomers in two directions of dissociation: parallel to the bilayer surface (lateral displacement) and parallel to the membrane normal (axial separation). These two computations are described below:

Lateral Displacement. Initial configurations for the sequence of umbrella sampling MD simulations were generated by performing COM distance constrained MD simulations. The distance between COMs of the two gA monomers parallel to the bilayer surface, denoted by R_{lat}, was changed with time from 0 to 2.2 nm, spanning configurations from the bound dimer to its dissociated monomers. Initial configurations were extracted as a grid of R_{lat} spacing 0.05 nm. At each grid point, the system was first equilibrated for 1 ns time period by freezing all atoms in the gA dimer in order to provide more time for the lipid to settle around the shifted gA monomers. Equilibrated configurations were then used as initial configurations for MD simulations with harmonic potentials that keep the R_{lat} near the desired values. The force constant of harmonic biasing potential was chosen as 8 kcal mol^{-1} Å^{-1} which ensures adequate overlap between the windows. Note that, change of the distance between COMs of the two gA monomers in the z direction is allowed during each window, since the z component of the distance between COMs of the two gA monomers was not constrained. In addition, directional changes of the R_{lat} were also allowed. In other words, monomers were able to rotate around each other with respect to the z axis. To ensure convergence, all MD simulations were run up to 10 ns.

Axial Separation. To obtain initial configurations for the sequence of umbrella sampling MD simulations along the direction of the membrane normal, MD simulation was performed with COM distance constraint of gA dimer that changes distance between COMs of two monomers parallel to the membrane normal (z component of the COM distance) denoted by R_{axial}

dx.doi.org/10.1021/jp2084583 |J. Phys. Chem. B XXXX, XXX, 000–000

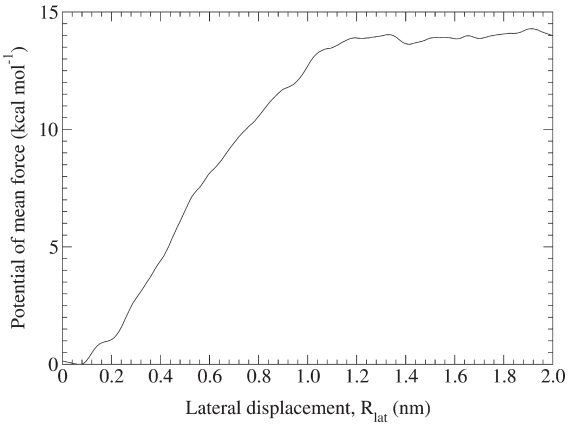

Figure 1. Potential of mean force as a function of lateral displacement.

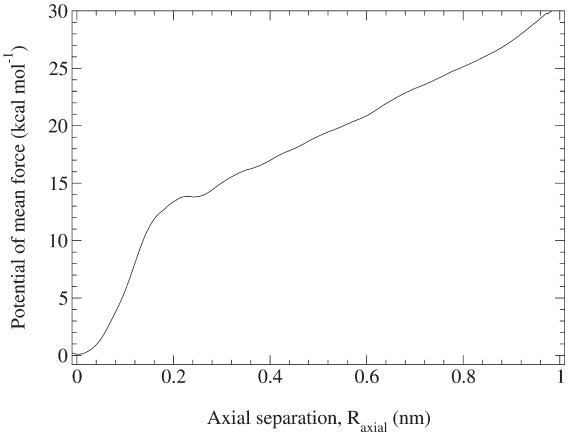

Figure 2. Potential of mean force as a function of axial separation.

from 1.38 to 2.38 nm. Initial configurations were extracted as a grid of R_{axial} spacing 0.02 nm. These configurations were equilibrated for a 1 ns time period. For each umbrella window, MD simulations were performed for 10 ns by constraining R_{axial} using a harmonic biasing potential with a force constant of 9 kcal mol^{-1} Å^{-1}. In each window, changes of the distance between COMs of the two gA monomers in xy-plane were allowed.

In both the lateral displacement and the axial separation, the force constant was chosen by several trial runs with different force constant to ensure an overlap of the configuration space explored in each window while also ensuring the configurations be adequately localized in each window. The chosen value was found to be optimal value among those trial values. Note that R_{lat} and R_{sep} were set to 0 when the two monomers form a dimer.

An additional term is required in specifying PMF if the chosen reaction coordinate function is nonlinear in the Cartesian coordinates. This additional term (Jacobian correction term) depends on the determinant of the Jacobian matrix that defines the transformation of the 3N Cartesian coordinates.[31] In this study, the Jacobian correction term is negligible since the reaction coordinate is linear in the axial separation, and approximately linear in the lateral displacement.

RESULTS

Figures 1 and 2 illustrate the PMF profiles of a gA dimer as functions of lateral displacement and axial separation, respectively.

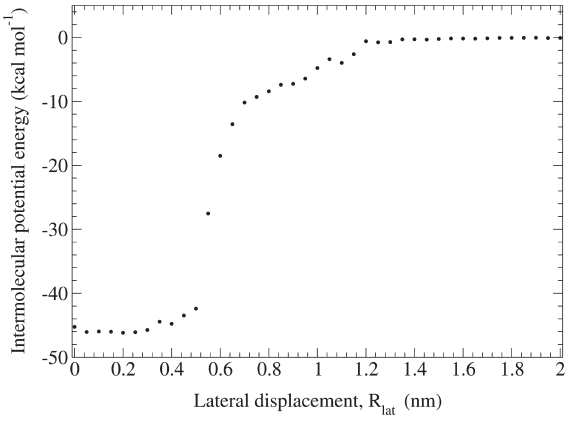

Figure 3. Intermolecular potential energies as a function of lateral displacement. Error bars in this and Figure 4 are not shown, as they are smaller than the data points.

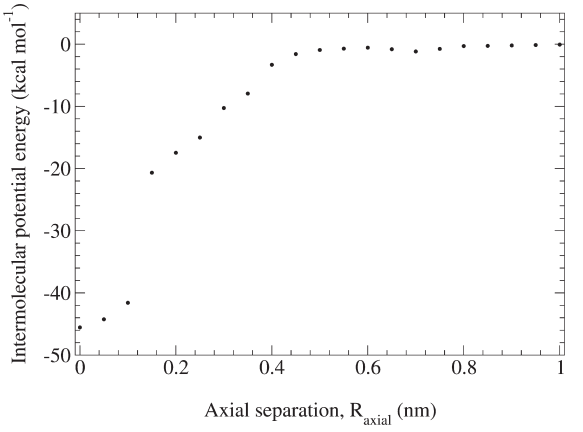

Figure 4. Intermolecular potential energies as a function of axial separation.

For the WHAM analysis, data from the first 1 ns of MD runs was disregarded to omit transient behavior. It is important to mention here that the PMF profiles converged well within the simulated time period of 10 ns in both directions. The error in the PMF was estimated by using 3 different portions of the overall time-series data collected over the umbrella sampling simulations (1−5, 1−7.5, and 1−10 ns). It was found that the error in the binding free energy is on the order of 1 kcal mol^{-1}. By examining the two PMF profiles (Figures 1 and 2), a significant bound dimer state can be observed, implying that the gA dimer is stable in the DMPC bilayer.

It is important to investigate how intermolecular potential energy between the two gA monomers change with the lateral displacement and the axial separation of monomers because of their physical relevance to the dissociation process. The intermolecular potential energy (sum of intermolecular electrostatic and Lennard-Jones potential energy between the two gA monomers) was obtained from the Charmm potential function at 0.01 ps time intervals in each umbrella window. For the lateral displacement, energy was separated according to the R_{lat} in intervals of 0.05 nm by including all trajectories obtained from window MD simulations. At each interval, the intermolecular potential energy was averaged and these averaged energy was plotted against the lateral displacement (Figure 3). Above steps were repeated for the axial separation and the intermolecular potential energy against the axial separation is shown in Figure 4.

dx.doi.org/10.1021/jp2084583 |J. Phys. Chem. B XXXX, XXX, 000–000

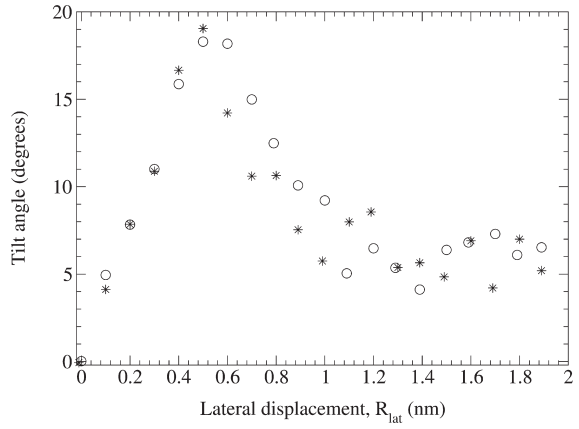

Figure 5. Tilt angles of two monomers as a function of lateral displacement.

In order to investigate gA dimer orientation during the lateral displacement, tilt angles with respect to the lipid bilayer normal (z axis) as a function of lateral displacement were calculated for both monomers and the results are shown in Figure 5. Helical axis vector was defined by connecting centers of masses of top and bottom backbone rings of the gA monomer. Tilt angle was calculated at 0.1 ps time intervals in each umbrella window. Average tilt angles at intervals of 0.1 nm were obtained by following the procedure used in averaging intermolecular potential energy. Tilt angles are set to zero at the ground state of the dimer. As R_{lat} increases, tilt angles of both gA monomers first increase at a same rate up to 0.5 nm of R_{lat}. After 0.5 nm of R_{lat}, tilt angles start to decrease up to 1.2 nm of R_{lat}. Afterward, they remain between 4 and 8 degrees instead of orienting along lipid bilayer normal. This result is also supported by an experiment conducted by Mo et al.[32] where it is suggested that the closed state of gA is not well oriented while the open state is well-oriented and structured in biological membranes.

When considering the lateral displacement of monomers (Figure 1), the PMF first increases with the increase of R_{lat} and then it reaches a plateau at about 1.2 nm. The flat area indicates that there is no free energy change with the change of R_{lat} in this region. This behavior makes intuitive sense, since after the dissociation of a dimer, the interaction between two monomers are zero. This result indicates that the dimer completely dissociates at $R_{la\ t} \approx$ 1.2 nm. Moreover, intermolecular potential energy in Figure 3 approaches to zero after 1.2 nm. Figure 6 gives snapshots of two gA monomers at different stages of intermolecular separation. The snapshots were produced using the UCSF Chimera package.[33] Based on the PMF in Figure 1, the energy gap between ground state gA dimer and dissociated monomers is ~14 kcal mol^{-1}.

In the axial separation, it can be seen in Figure 2 that the PMF increases with intermolecular separation. However, the PMF does not reach a maximum value within the simulated range of R_{axial}. By examining the PMF curve in Figure 2, it can be seen that PMF increases linearly after approximately 0.26 nm of R_{axial}. From Figure 4, it can be seen that intermolecular potential energy becomes zero at about 0.5 nm of distance of separation from the equilibration distance. Even though this is the case, most of the intermolecular potential energy increase (~90%) occurs before 0.4 nm of R_{axial}. Although the intermolecular interaction energy between gA monomers become zero after the breaking of all

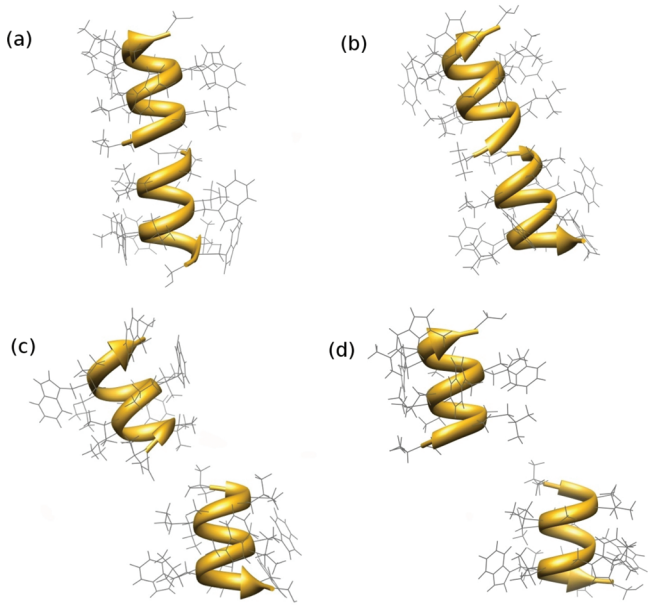

Figure 6. Snapshots of the gA dimer at the different R_{dis} in lateral displacement (a) ground state, (b) 0.4, (c) 0.7, and (d) 1.2 nm.

noncovalent bonds, the PMF in Figure 2 increases with the increase of COM distance. The reason for this is that when COM distance increases, the hydrophobic part of the gA monomer gradually enters the water layer resulting in an increase in the energy of the system. If one extends the PMF curve by changing R_{axial} until both monomers completely leave the DMPC bilayer, then the PMF curve will plateau. In other words, after the gA monomers completely move into water, the intermolecular interaction energy involving gA monomers remains approximately the same, regardless of the R_{axial}. Furthermore, linear energy increases after 0.26 nm implying that the PMF increase after this distance is mainly due to the hydrophobic effect. On the other hand, 0.26 nm is approximately equal to the hydrophobic mismatch (difference in the hydrophobic lengths of the gA dimer (~2.2 nm[11]) and the surrounding DMPC bilayer (~2.48 nm at 313 K[34])). The dissociation energy from Figure 2 is then ~14 kcal mol^{-1}, which is the PMF change within 0.26 nm of separation.

DISCUSSION

The PMF and intermolecular potential energy of a gA dimer as functions of lateral displacement and axial separation are computed via MD simulations. First, consider the axial separation of monomers. Figure 4 shows that intermolecular potential energy increases rapidly at the beginning of the axial separation. Moreover, 90% of the energy increase happens within 0.4 nm, indicating that all noncovalent bonds break approximately within this distance. On the other hand, breaking noncovalent bonds increases the monomers' flexibility that leads to increase of monomers' entropy. However, Figure 2 shows that the PMF increases with the axial separation, suggesting that the contribution of energy increase due to the bond breaking is larger than that of energy decrease due to the entropy gain.

Next, consider the behavior of intermolecular potential energy profiles with the lateral displacement of gA monomers (Figure 3). At the beginning of the lateral displacement, intermolecular potential

dx.doi.org/10.1021/jp2084583 |J. Phys. Chem. B XXXX, XXX, 000–000

energy stays approximately constant until 0.5 nm of R_{lat}, indicating that noncovalent bonds in the gA dimer remain virtually unchanged at this R_{lat} region. In order to maintain noncovalent bonds while R_{lat} increases, the entire dimer tilts with respect to the bilayer normal. In other words, tilting of dimers allows increasing of the R_{lat} without breaking noncovalent bonds between the gA monomers. Figure 5 shows that both monomers tilt at the same rate and also the sine of tilt angle and R_{lat} is proportional in this region, confirming that the increase of the R_{lat} achieves through the tilting of dimer. A snapshot of the dimer at 0.4 nm of R_{lat} is shown in Figure 6b. Even though intermolecular energy stays constant in this region of R_{lat}, PMF increases with the increase of R_{lat} (Figure 1). Tilting of dimers shifts the lipids adjacent to the channel and dimer start to experience a lateral resistance from the surrounding lipid that reduces the degrees of freedom (flexibility) of dimers and thereby, decreases the entropy of dimers. As a result, the free energy of dimers increases as illustrated in Figure 1.

With the further increase of R_{lat}, the tilting of dimers is no longer able to overcome increasing lateral resistance from the surrounding lipid molecules. Therefore, noncovalent bonds start to break with the increase of the R_{lat} as illustrated by Figure 3, which shows increasing of intermolecular potential energy after 0.45 nm of R_{lat}. Specifically between 0.5 and 0.7 nm of R_{lat}, the intermolecular potential energy increases dramatically. This indicates breaking of several noncovalent bonds within a short-range of R_{lat}. Furthermore, snapshot of the gA dimer at 0.7 nm of R_{lat} shown in Figure 6c illustrates that one monomer tilts relatively to the other monomer. This behavior can also be seen in Figure 5 which shows that one monomer's tilt angle starts to decrease 0.1 nm later in R_{lat} than the other monomer's tilt angle. Relative tilting of one monomer aids the other monomer to reorient along bilayer normal while increasing the R_{lat}. As a result of this relative tilting, several noncovalent bonds break and intermolecular energies increase. In this case, degrees of freedom of gA monomers increase and thereby, gA dimers gain entropy with the breaking of intermolecular noncovalent bonds. However, Figure 1 shows an increase of the PMF, suggesting that the energy increase due to the bond breaking is larger than the energy decrease due to the entropy gain.

Recall the behavior of the PMF (Figure 2) and the intermolecular potential energy (Figure 4) at the beginning of the axial separation. Both the intermolecular energy and the PMF show rapid increase when intermolecular bonds break. Intermolecular potential energy in the lateral displacement (Figure 3) also shows same type of increase when bonds break. However, the PMF in the lateral displacement (Figure 1) does not show rapid increase as seen in the PMF in the axial separation (Figure 2). This is due the fact that the gaining of the entropy with the breaking of bonds in the lateral separation is not only from breaking of bonds but also from regaining the flexibility of dimers. As a result, the slope of the PMF decreases. Finally, with further increase of the R_{lat}, potential energy continues to increase and gradually become zero where the complete dissociation occurs.

As discussed above, the dissociation by lateral displacement is an incremental process whereas the dissociation by axial separation is a rapid one step process. Furthermore, comparison of the slopes of two PMFs shows that the slope at the beginning of the axial separation (Figure 2) is approximately 6 times lager than the slope at the beginning of the lateral displacement (Figure 1). This implies that in order to dissociate the gA dimer in the axial direction, it is necessary to supply dissociation energy instantaneously. More importantly, the energy required to separate monomers by 0.2 nm from the ground state dimer is ~14 kcal mol^{-1}. Furthermore, experimental results show existence of several intermediate states of gA channels in addition to their conventional open and close states.[15,16] By considering these facts, it can be concluded that the gA dimer dissociates with lateral displacement rather than a direct axial separation.

CONCLUSIONS

The conclusion then is that the gA dimer dissociation in the lipid bilayer is an incremental process rather than a rapid one step dissociation. With the internal energy increase, dimers first tilt until the resistive forces from the surrounding lipids becomes stronger than the rotation force. Then, dimers start to dissociate by breaking several intermolecular noncovalent bonds where one monomer tilts relatively to the other monomer. Interaction between monomers becomes weak with breaking of number of noncovalent bonds and hence complete dissociation occurs. Furthermore, the dissociation energy of the gA dimer in the DMPC bilayer is found to be ~14 kcal mol^{-1}. Given that each intermolecular hydrogen bond has ~2.4 kcal mol^{-1} of dissociation activation energy,[35] 14 kcal mol^{-1} reflects the energy to break the 6 intermolecular hydrogen bonds of the gA dimer. It is also found that the open state of gA is well oriented along the lipid bilayer normal and the close state is not well oriented.

AUTHOR INFORMATION

Corresponding Author

*Telephone: (604) 822 2653. E-mail: vikramk@ece.ubc.ca.

ACKNOWLEDGMENT

This work was supported by grants from the Natural Sciences and Engineering Research Council (NSERC) of Canada and the MAWA Trust. All computations were performed using computing resources provided by WestGrid (www.westgrid.ca) and Compute/Calcul Canada. We thank Dr. Mark Thachuk (Chemistry, University of British Columbia) for his valuable suggestions and comments.

REFERENCES

(1) Hille, B. *Ion Channels of Excitable Membranes*; Sinauer Associates Inc.: Sunderland, 1992.

(2) Krishnamurthy, V.; Monfared, S. M.; Cornell, B. *IEEE Trans. Nanotechnol.* **2010**, *9*, 303–312.

(3) Urry, D. W. *Proc. Natl. Acad. Sci. U.S.A.* **1971**, *68*, 672–676.

(4) Ketchem, R. R.; Hu, W.; Cross, T. A. *Science* **1993**, *261*, 1457–1460.

(5) Koeppe, R. E.; Killian, J. A.; Greathouse, D. V. *Biophys. J.* **1994**, *66*, 14–24.

(6) Arseniev, A. S.; Lomize, A. L.; Barsukov, I. L.; Bystrov, V. F. *Biol. Membr.* **1986**, *3*, 1077–1104.

(7) Townsley, L. E.; Tucker, W. A.; Sham, S.; Hinton, J. F. *Biochemistry* **2001**, *40*, 11676–11686.

(8) Bamberg, E.; Läuger, P. *J. Membr. Biol.* **1973**, *11*, 177–194.

(9) Wallace, B. A. *Annu. Rev. Biophys. Biophys. Chem.* **1990**, *19*, 127–157.

(10) Koeppe, R. E.; Anderson, O. S. *Annu. Rev. Biophys. Biomol. Struct.* **1996**, *25*, 231–258.

(11) Elliott, J. R.; Needham, D.; Dilger, J. P.; Haydon, D. A. *Biochim. Biophys. Acta, Biomembr.* **1983**, *735*, 95–103.

(12) Sandblom, J.; Galvanovskis, J.; Jilderos, B. *Biophys. J.* **2001**, *81*, 827–837.
(13) Ring, A. *Biophys. J.* **1992**, *61*, 1306–1315.
(14) Goulian, M.; Mesquita, O. N.; Fygenson, D. K.; Nielsen, C.; Andersen, O. S.; Libchaber, A. *Biophys. J.* **1998**, *74*, 328–337.
(15) Harms, G. S.; Orr, G.; Montal, M.; Thrall, B. D.; Colson, S. D.; Lu, H. P. *Biophys. J.* **2003**, *85*, 1826–1838.
(16) Lu, H. P. *Acc. Chem. Res.* **2005**, *38*, 557–565.
(17) Miloshevsky, G. V.; Jordan, P. C. *Biophys. J.* **2004**, *86*, 92–104.
(18) Miloshevsky, G. V.; Jordan, P. C. *Structure* **2006**, *14*, 1241–1249.
(19) Torrie, G. M.; Valleau, J. P. *Chem. Phys. Lett.* **1974**, *28*, 578–581.
(20) Ketchem, R. R.; Lee, K. C.; Huo, S.; Cross, T. A. *J. Biomol. NMR* **1996**, *8*, 1–14.
(21) Jo, S.; Kim, T.; Iyer, V. G.; Im, W. *J. Comput. Chem.* **2008**, *29*, 1859–1865.
(22) Foloppe, N.; MacKerell, A. D., Jr *J. Comput. Chem.* **2000**, *21*, 86–104.
(23) Jorgensen, W. L.; Chandrasekhar, J.; Madura, J. D.; Impey, R. W.; Klein, M. L. *J. Chem. Phys.* **1983**, *79*, 926–935.
(24) Nosé, S. *Mol. Phys.* **1984**, *52*, 255–268.
(25) Hoover, W. G. *Phys. Rev. A* **1985**, *31*, 1695–1697.
(26) Parrinello, M.; Rahman, A. *J. Appl. Phys.* **1981**, *52*, 7182–7190.
(27) Chiu, S. W.; Clark, M.; Balaji, V.; Subramaniam, S.; Scott, H. L.; Jakobsson, E. *Biophys. J.* **1995**, *69*, 1230–1245.
(28) Berendsen, H. J. C.; van der Spoel, D.; van Drunen, R. *Comput. Phys. Commun.* **1995**, *91*, 43–56.
(29) van der Spoel, D.; Lindahl, E.; Hess, B.; Kutzner, C.; van Buuren, A. R.; Apol, E.; Meulenhoff, P. J.; Tieleman, D. P.; Sijbers, A. L. T. M.; Feenstra, K. A.; van Drunen, R.; Berendsen, H. J. C. *Gromacs User Manual version 4.0*; University of Groningen: Netherlands, 2005.
(30) Kumar, S.; Bouzida, D.; Swendsen, R. H.; Kollman, P. A.; Rosenberg, J. M. *J. Comput. Chem.* **1992**, *13*, 1011–1021.
(31) Trzesniak, D.; Kunz, A.-P. E.; van Gunsteren, W. F. *ChemPhysChem* **2007**, *8*, 162–169.
(32) Mo, Y.; Cross, T. A.; Nerdal, W. *Biophys. J.* **2004**, *86*, 2837–2845.
(33) Pettersen, E. F.; Goddard, T. D.; Huang, C. C.; Couch, G. S.; Greenblatt, D. M.; Meng, E. C.; Ferrin, T. E. *J. Comput. Chem.* **2004**, *25*, 1605–1612.
(34) Petrache, H. I.; Dodd, S. W.; Brown, M. F. *Biophys. J.* **2000**, *79*, 3172–3192.
(35) Huang, H. W. *Biophys. J.* **1986**, *50*, 1061–1070.